Absolute Characterization of Gravity Sag for Light-Weighted Optics

Tomasz Lis, Stephen Cheney, H. Philip Stahl

NASA MARSHALL SPACE FLIGTH CENTER, HUNTSVILLE, AL 35812

ABSTRACT

Gravity-sag (G-sag) for large space-based telescopes is a critical error budget element that must be taken in consideration. Absolute characterization of gravity sag provides necessary information when testing light weighted optics so that true optical performance can be determined. A method is presented for characterizing G-sag to obtain the 0-G optical surface.
Keywords: wavefront error, gravity sag, space telescopes, light-weighted mirror, optical test

1. INTRODUCTION

Missions such as Webb, the Roman space telescope or a future 6-meter telescope need to polish mirrors such that their zero-gravity surface figure meets the required science drive performance specification. [1]. For space telescopes to perform UV science (i.e. diffraction limited at < 500 nm), being able to characterize a mirror's surface figure to within 2 nm RMS is essential because for a UV/Optical telescope the G-release needs to be less than 4 nm RMS. The Astrophysics 2020 Decadal identified quantifying and mitigating gravity-sag as a critical technology need [1]. This work also maps to the 2022 Astrophysics Biennial Technology Report by developing analysis techniques that support Mirror Technologies for High Angular Resolution (UV/Vis/Near-IR) [4].

2. Gravity Sag Analysis

This paper describes a preliminary effort to demonstrate the ability to estimate gravity sag and quantify the uncertainty of that estimate to an accuracy of < 2 nm RMS. For this effort, we are using mirrors whose stiffness is such that they have substantial amount of gravity sag [1]. For horizontal testing, we are using the Evans and Kestner 'N-rotation" algorithm where a mirror is measured with an interferometer for N-rotation angles i.e. N=3 (0°, 120°, 240°) or N=6 (0°, 60°, 120°, 180°, 240°, 300°) [2]. Averaging the rotations removes test errors with angular dependance up to (N-1), i.e. N=3 will remove coma, secondary coma, tertiary coma, etc.; and, astigmatism, secondary astigmatism, tertiary astigmatism, etc.) [1]. In a horizontal test condition, the gravity sag is asymmetric which is why performing a rotation test can determine the gravity sag and allow for it to be removed from the measurement of the surface figure [1]. The surface figure of the mirror can be decomposed into the following; rotationally symmetric components, rotationally asymmetric components and the gravity sag.

$$S(x,y,\theta_i)_{Horizontal} = \left[S(x,y)_{G(0,0,0)_{symmetric}} + S(x,y,\theta_i)_{G(0,0,0)_{asymmetric}}\right] + S(x,y,\theta=0)_{G(0,-1,0)} \quad (1)$$

Where the surface normal is pointed in the z-direction and gravity is pointed in the -1 Y (G(0,-1,0)) direction. With the mirror rotated in angles of theta around its surface normal only the asymmetric components of the mirror will rotate. Thus, the gravity sag will not rotate nor will the rotationally symmetric components, so averaging the rotations results in only the mirror's symmetric surface shape and its gravity sag being left which results in the following equation [1].

$$\frac{1}{N}\sum_{i=0}^{N-1} S(x,y,(\theta_i = 360(i/N)))_{Horizontal} = S(x,y)_{G(0,0,0)_{symmetric}} + S(x,y,\theta=0)_{G(0,-1,0)} \quad (2)$$

To get the predicted zero-G surface shape, the measured data is back-rotated to theta=0 and averaged. This removes the non-rotationally gravity sag terms, leaving the following terms [1].

$$\frac{1}{N}\sum_{i=0}^{N-1} S(x,y,(\theta_i = 0)_{Horizontal} = \left[S(x,y)_{G(0,0,0)_{symmetric}} + S(x,y,\theta_i)_{G(0,0,0)_{asymmetric}}\right] \quad (3)$$

Following the method described above allows for the G-sag to be removed for the mirror's measured surface figure [1]. The gravity sag can be determined by subtracting the results of Equation 3 from the raw data taken which would leave only the G-sag term.

2.1 Experimental Setup

The mirror assembly is attached to a rotation stage that can rotate the mirror with an ~1 arcsecond accuracy. The rotation stage is mounted to a hexapod which allows for fine alignment of the mirror to the optical axis. At the mirror's center of curvature is a 4D interferometer mounted on a hexapod. The hexapod allows for fine alignment of the interferometer to the optical axis of the mirror. An example of the setup for this testing is shown in the top image of Figure 1 with the mirror and its mounting structure setup inside the vacuum chamber and the interferometer attached to a tripod outside of the chamber. The light-weighted back structure of the mirror with its three mounting points is shown in the bottom image of Figure 1.

Most of the gravity sag testing is done in a 1 m vacuum chamber set at ambient pressure and temperature to test smaller mirrors with short ROC. There are also two large chambers that can accommodate larger mirrors with longer ROC with one of the larger chambers being shown in Figure 1.

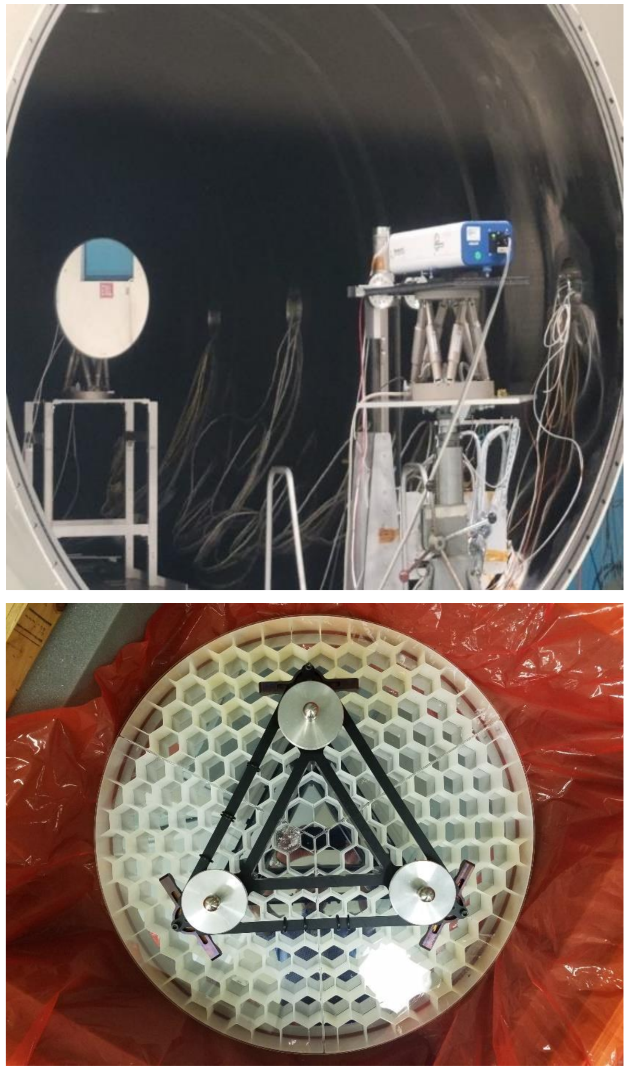

Figure 1: *DOT mirror testing in the SLTF on top and image of mirror back structure on bottom.*

2.2 Gravity Sag Testing

To test the gravity sag, a light-weighted mirror with a diameter of 0.6m and a ROC of 5m was used. The mirror was tested multiple times with each test having the mirror rotated N=6 times which removed up to N-1 rotational errors which includes coma, astigmatism, trefoil, etc. For each of these tests the 0-G and gravity sag were determined by the following method.

1. Collect all raw unprocessed data from the horizontal rotation test.
2. Remove tip/tilt and piston from each of the data points.
3. Back rotate the data so that each data point is aligned.
4. Average the rotated data which will remove the gravity sag and any rotationally symmetric errors up to N-1 Theta and leaves the 0-G figure and the rotationally asymmetric terms [1].
5. Subtracting the step 4 data (0-G/rotationally asymmetric terms) from the back rotated data will leave only the G-sag term.

In Figure 2, the results of steps described above can be seen with the left phase map showing the as measured surface shape for the 0 degree rotation, the middle phase map showing the 0-G surface estimate, and the right phase map showing the gravity sag for the 0 degree rotation. For this test the gravity sag ranges from 102-125 nm RMS. G-sag is mostly astigmatism ranging from 246-308 nm PV.

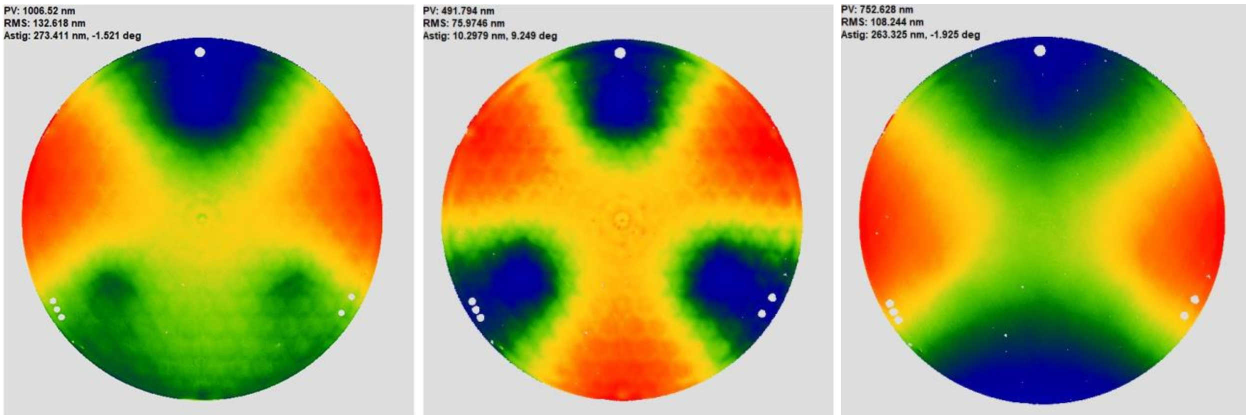

Figure 2: Left phase map is of an unprocessed measurement from the 4D interferometer. The middle phase map is of the 0-G surface of the mirror under test. The right phase map is of the gravity sag of the phase map on the left.

To test the reproducibility the mirror was tested several times with the mirror being removed from its mount and then reattached. For each of these measurements the same procedure described above was performed to determine the 0-G figure. For three of these measurements the 0-G data was subtracted from a fourth 0-G measurement. The difference data between these measurements is shown in Figure 3 with the RMS values ranging from 2.8nm-8.0nm. Please note that these tests were performed in ambient atmospheric conditions.

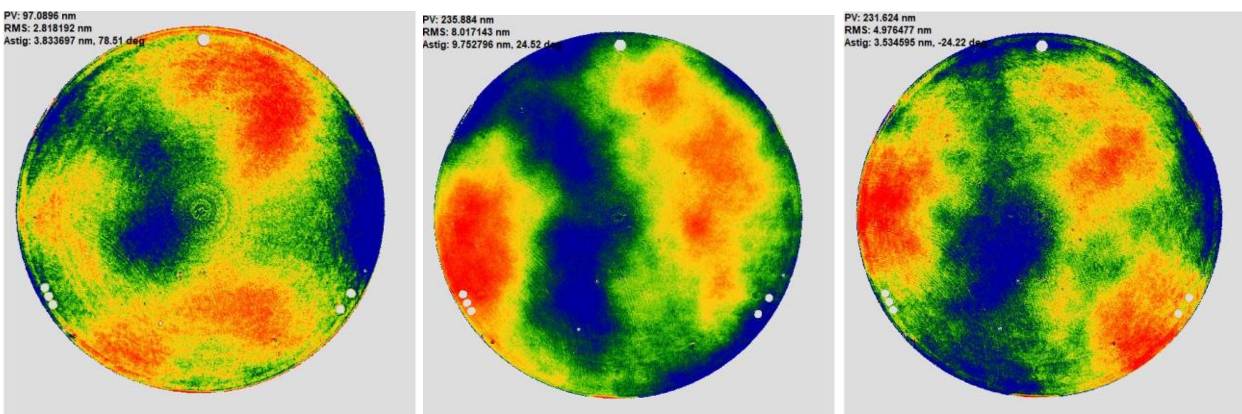

Figure 3: Phase map differences between one rotation test and three separate data sets to determine reproducibility.

To determine the uncertainty in the gravity sag estimate the gravity sag measurements are back-rotated to the theta=0 positions for all the measured data so that the data is aligned. When the back-rotated gravity sag measurements are averaged the gravity sag averages out of the measurements where the gravity sag is orthogonal (as shown in Figure 4) and the only term remaining is the residual error left from the measurement.

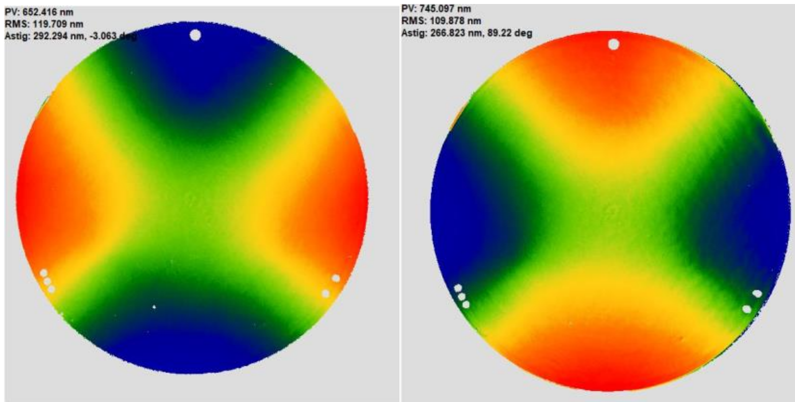

Figure 4:Back-rotated gravity sag for two orthogonal measurements with the left phase map being a 0-degree rotation and the right phase map being a 180-degree rotation measurement.

The uncertainty for a single G-sag estimate of the DOT mirror is shown in the left data of Figure 5 and has an RMS value of ~3.6 nm. The right phase map of Figure 5 shows the difference between the uncertainty phase maps of two separate data sets. The possible sources for the uncertainty can come from multiple sources such as: mis-registration shear error of pocket quilting, variation in pocket quilting, mount pad deflection as a function of rotation, etc. The error seen in Figure 5 is from limitations of registration from the 4D and shear effects from bending of the substrate and mount.

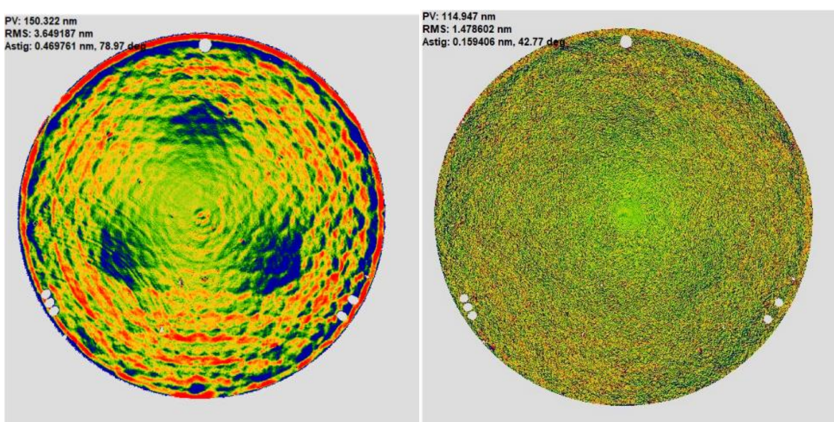

Figure 5: In the left the Phase map of the DOT mirror's gravity sag uncertainty for one of the data sets. The right image shows the difference between the uncertainty phase maps of two data sets.

It is important to note that the gravity sag uncertainty is mostly mid-spatial frequency. As shown in Figure 6 the PSD of the uncertainty of the G-sag has noticeable mid-spatial frequency structure. In the bottom graph of Figure 6 is the PSD for the difference between the uncertainty of two data sets. The "bumps" seen in the top graph have disappeared which means that the mid-spatial bumps seen are repeatable and present in the mirror itself so when the gravity sag phase map is calculated by removing the 0-G phase map some asymmetric components are left in the gravity sag phase maps. This is due to the back rotation used to calculate the 0-G phase map which was described in section 2. And, it is important to note that the uncertainty in the estimate of the low-order gravity sag terms, including astigmatism, is very good – less than 1 nm rms.

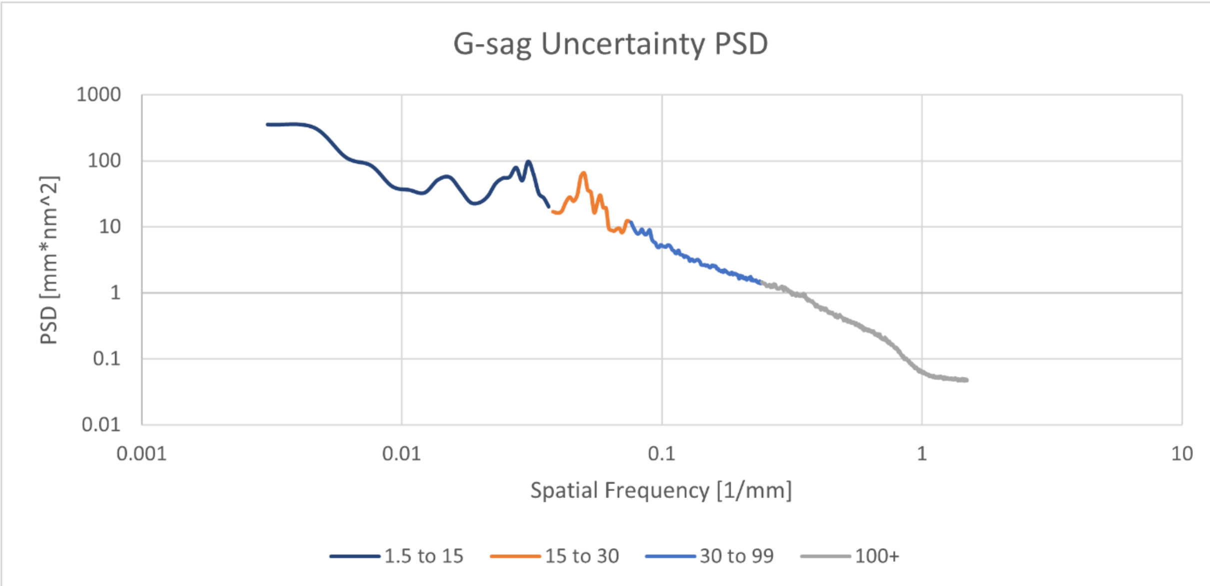

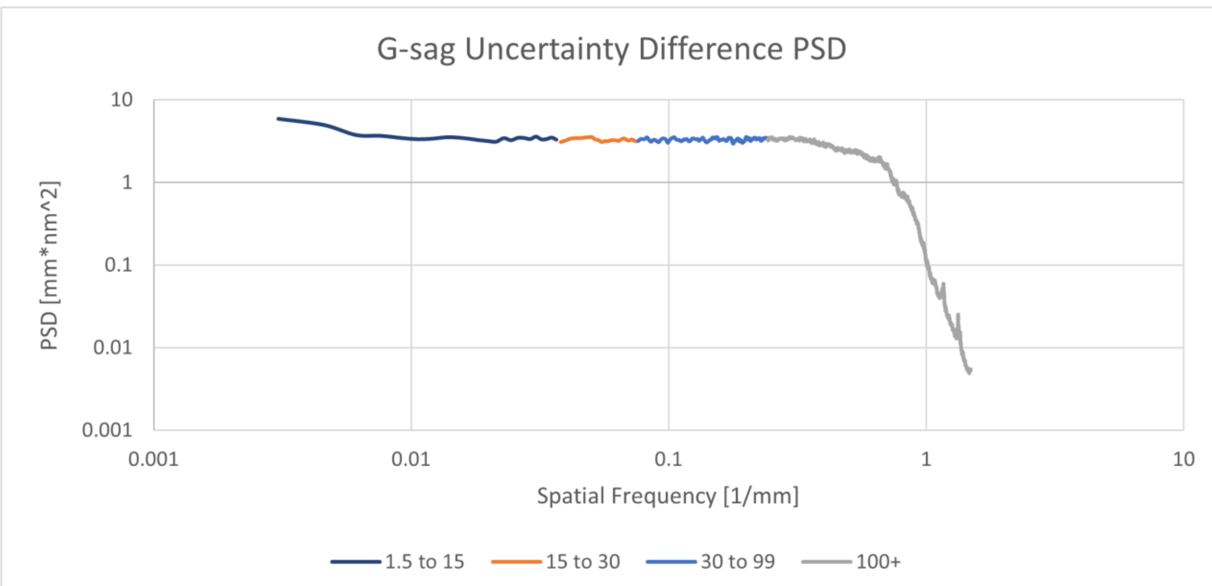

Figure 6: A map of the uncertainty for the G-sag of the DOT mirror is shown on the top and the PSD of the G-sag uncertainty is shown on the bottom

2.3 Error in Angle Positoning

To determine how much a misalignment in rotation angle affects the results when calculating the 0-G a mirror was rotated to three “misaligned” rotations from the 0 degree position (θ= 1, 2, 5 degrees) with a N=6 rotation test being performed as well.

The process described in section 2 was then employed to determine what the 0-G surface figure was for each of the three rotations plus the 0-G of the aligned rotation. The calculated 0-G data from the three misaligned positions was then subtracted from the aligned 0 degree 0-G surface figure which provides a data map of the leftover errors. The results of these differences is shown in the phase maps of Figure 7. As can be seen in the phase maps below as the misalignment angle increases the phase maps have more shear between the pockets in the backplane. This shear in turn increases the rms value from ~2.2 nm at 1 degree misaligned to ~6.0 nm at 5 degree misaligned. Note that the 1-degree rotation error is similar in form and magnitude to the reproducability experiment.
At small misalignments the RMS does not change substantially but as the misalignment angle increases the RMS increases. This would yield confidence that at misalignment angles less than 1 degree there are not substantial error contributions but if the error need to be quantified in the 4 nm range such as in a HabEx flagship mission this would consume almost 50% of the error budget [3].

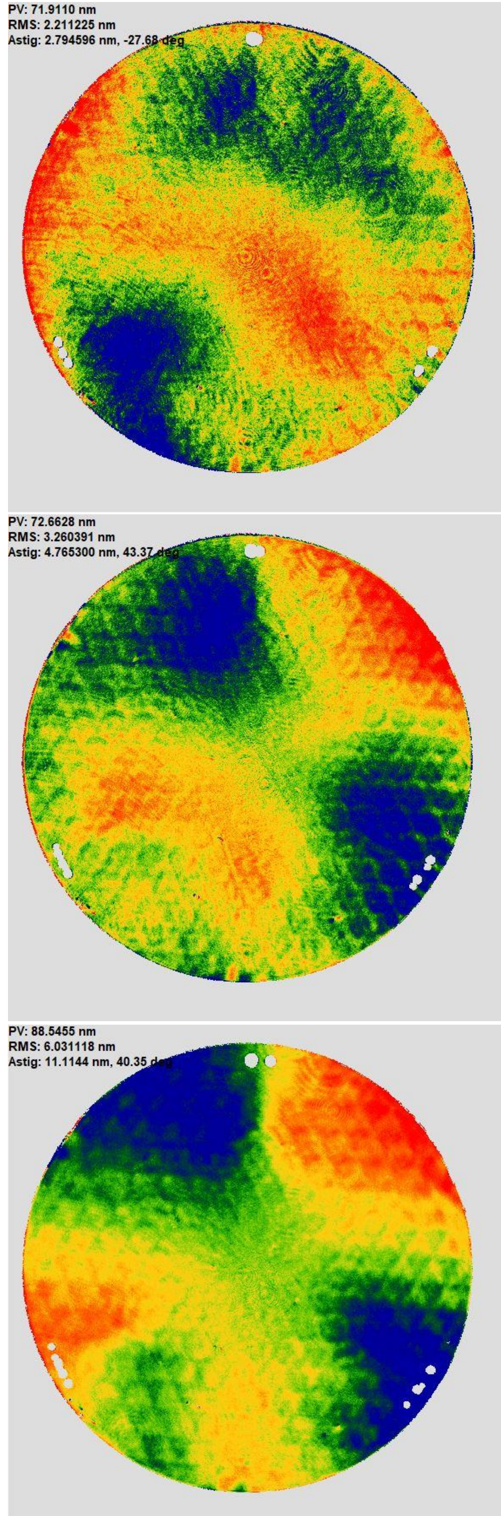

Figure 7: Difference between the aligned zero gravity surface figure and the zero gravity surface figure with one of the data points rotationally misaligned. The top phase map shows the difference between the aligned zero gravity phase map and the zero gravity phase map with one measurement misaligned by 1 degree. The middle phase map shows the difference between the aligned zero gravity phase map and the zero gravity phase map with one measurement misaligned by 2 degrees. The bottom phase map shows the difference between the aligned zero gravity phase map and the zero gravity phase map with one measurement misaligned by 5 degrees.

2.4 Modeling Gravity Sag

As space mirrors get larger, their gravity sags also get larger. An enabling technology for designing and manufacturing large space mirrors are validated modeling tools for predicting gravity sag. Understanding how to remove the G-sag error from the measurement of the surface figure produces a map of the surface performance in space. Some results of the testing are shown in Figure 8 with a map of the gravity sag in its “0-deg” orientation shown and a model of the predicted gravity sag shown as well.

CAD models were made of the mirror using Creo and Finite Element analysis was conducted using Ansys. Standard RMS normalized Zernike polynomials via SigFit software were used to fit the surface after the disturbance case. (Chosen to agree with 4D interferometer standard output) A variety of meshing techniques and sizes were used in order to confirm convergence of the deformed shape. Computer generated predictions greatly differ from measured data. A summary of the first few Zernike terms can be seen in Table 1. Current assumptions are that the computer modeled geometry does not accurately account for the post slumped geometry of the physical mirror. See future work section below for future efforts to investigate these discrepancies.

Table 1: Summary of measured RMS Zernike terms vs computer generated RMS Zernike estimates.

	Measured (nm)	comp estimated (nm)
astg X	291	202
astg Y	-31	-0.1
coma X	4.6	-0.1
coma Y	27.3	3.7
pri Sphere	-2	-0.1
Tre X	0.7	0.05
Tre Y	0.8	-0.02
2nd astg X	-50.6	-25.1
2nd astg Y	9.7	0.05
2nd coma X	12.9	0.05
2nd coma Y	-4.7	1.1

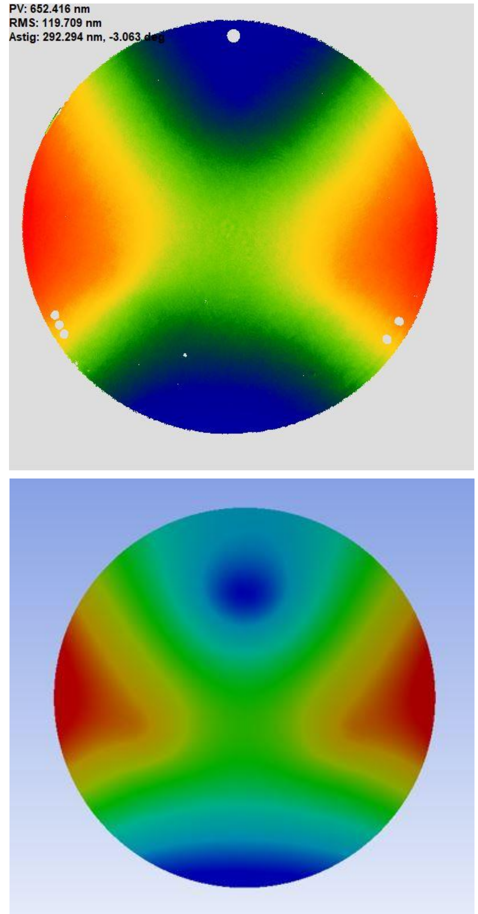

Figure 8: model of the predicated G-sag for the DOT mirror on the left and the actual measured G-sag on the right.

3. CONCLUSIONS AND FUTURE WORK

G-release is a critical component of the error budget when designing a telescope for a low gravity environment. This paper has described a method for estimating a mirror’s zero-gravity surface figure and uncertainty. By doing the A 60-cm 80-Hz mirror was tested using the horizontal rotation method and shown to have a gravity sag from 102-125 nm RMS with an uncertainty of < 3.8 nm RMS (< 1 nm rms for low-spatial frequency).

More work can be done to further improve the characterization of the gravity sag and determination of the zero-gravity surface figure. For example, developing more accurate gravity sag models. Attempts to accurately portray the slumped mirror geometry will be made and other mirrors with simpler manufacturing processes, core geometries and mounting geometries are already being tested. This will help close the loop on making accurate predictive models which will allow for the use of a CGH to remove the gravity sag for mirrors that have gravity sag that exceed the working range of the interferometer. Work will also be done to further characterize the environmental errors and asymmetric errors that contribute to the uncertainty in the measurements. Over the next year, work will be done to test mirrors that have multiple microns of gravity sag and test them with CGH's as a proof of concept for larger flagship missions. Another avenue that will be explored is face-up/face-down testing of the mirror to compare the results from the horizontal rotation test method of determining the zero gravity surface figure. With all these steps taken we believe that the G-sag uncertainty specification of < 2 nm RMS can be achieved.

References

1. H. Philip Stahl "Absolute characterization of gravity sag", Proc. SPIE 11487, Optical Manufacturing and Testing XIII, 114871F (20 August 2020); https://doi.org/10.1117/12.2568795

2. Evans, Chris J., and Robert N. Kestner, "Test optics error removal", Applied Optics, Vol.35, No.7, pp.1015-21, 1 March 1996.

3. H. Philip Stahl, Gary Kuan, William Arnold, Mike Baysinger, Thomas Brooks, Jay Garcia, J. Brent Knight, "Habitable-zone observatory (HabEx) baseline 4-m telescope design and predicted performance," Proc. SPIE 11443, Space Telescopes and Instrumentation 2020: Optical, Infrared, and Millimeter Wave, 114433C (13 December 2020); https://doi.org/10.1117/12.2562879

4. Stahl, H. Philip, Rhonda Morgan, "Technology development roadmap for Habitable-zone exoplanet observatory (HabEx) baseline 4-m primary mirror," Proc. SPIE 11116, Astronomical Optics: Design, Manufacture, and Test of Space and Ground Systems II, 1111604 (9 September 2019);

5. Schulz, Gunter, "Absolute flatness testing by an extended rotation method using two angle of rotation", Applied Optics, Vol.32, No.7, pp.1055-59, 1 March 1993